A Very High Resolution General Circulation Model Simulation of the Global Circulation in Austral Winter

PHILIP W. JONES

Theoretical Division, Los Alamos National Laboratory, Los Alamos, New Mexico

KEVIN HAMILTON AND R. JOHN WILSON

Geophysical Fluid Dynamics Laboratory/NOAA, Princeton University, Princeton, New Jersey

(Manuscript received 3 July 1996, in final form 14 October 1996)

ABSTRACT

This paper discusses a simulation obtained with the Geophysical Fluid Dynamics Laboratory ''SKYHI'' troposphere–stratosphere–mesosphere general circulation model run at very high horizontal resolution (~60-km grid spacing) and without any parameterization of subgrid-scale gravity wave drag. The results are for a period around the austral winter solstice, and the emphasis is on the simulated Southern Hemisphere (SH) winter circulation. Comparisons are made with results obtained from lower horizontal resolution versions of the same model.

The focus in this paper is on two particularly striking features of the high-resolution simulation: the extratropical surface winds and the winter polar middle atmospheric vortex. In the extratropical SH, the simulated surface westerlies and meridional surface pressure gradients in the high-resolution model are considerably stronger than observed and are stronger than those simulated at lower horizontal resolution. In the middle atmosphere, the high-resolution model produces a simulation of the zonal mean winter polar vortex that is considerably improved over that found with lower resolution models (although it is still significantly affected by the usual cold pole bias). Neither the improvement of the middle atmospheric polar vortex simulation nor the deterioration of the simulation of surface winds with increased model resolution shows a clear convergence, even at the ~60-km grid spacing employed here.

1. Introduction

Despite the vast experience obtained over the last three decades with general circulation models (GCMs), some very fundamental issues in the area of first-principles comprehensive modeling of the atmosphere remain to be clarified. One problem that has appeared is a tendency for the low-level westerlies (and associated meridional surface pressure gradients) to increase significantly with improvements in the horizontal resolution of the models employed (e.g., Manabe et al. 1979; Boville 1991; Held and Phillips 1993). At sufficiently high horizontal resolution, GCMs will typically produce surface westerlies in the Northern Hemisphere (NH) winter that are much stronger than observed. A solution that has been adopted in many GCMs is to include a drag on the zonal flow ascribed to topographically forced gravity waves of subgrid-scale. With a plausible amount of such parametrized gravity wave drag (GWD), it appears that the simulated surface winds in the NH winter can be made realistic (Palmer et al. 1986; McFarlane 1987; Boer and Lazare 1988). In the Southern Hemisphere (SH), the effects of subgrid-scale gravity wave drag are likely to be rather insignificant, so it is of interest to see how the surface flow varies with resolution in SH winter. For at least some models (e.g., Manabe et al. 1979; Hamilton et al. 1995) it turns out to be possible to find a horizontal resolution that produces a realistic simulation of the SH winter surface winds and too-intense NH winter surface winds (which can then be adjusted with gravity wave drag). However, the question of what happens when resolution is increased beyond this comfortable range has not been widely addressed thus far. One exception is the work of Hamilton et al. (1995, hereafter HWMU), who performed integrations with a gridpoint GCM (without parameterized GWD) run at various horizontal resolutions. HWMU observed the familiar increase of surface westerlies with resolution in both the NH and SH winter. At the highest horizontal resolution considered by HWMU (~100-km grid spacing), the June–August climatology of the simulated SH surface winds was found to be stronger than observed (particularly in the circumpolar oceanic region).

Corresponding author address: Dr. Kevin Hamilton, GFDL/NOAA, P.O. Box 308, Princeton, NJ 08542.
E-mail: kph@gfdl.gov

Another major problem found in GCMs that include the middle atmosphere is a tendency for simulations above the tropopause to be too close to radiative equilibrium, notably with winter polar temperatures unrealistically low throughout the middle atmosphere. In the NH winter this polar cold bias seems to affect many GCM simulations to some extent, but there are some significant differences in the performance of various GCMs in this regard. HWMU found that their NH winter simulation (with no GWD parameterization) was characterized by a polar vortex that is somewhat too strong and definitely too narrowly confined near the pole, and that this is accompanied by a cold bias of ~10°–15°C in the lower mesosphere. Boville (1991) finds that his simulated NH polar temperatures are very much too cold (~50°C or more) unless he incorporates a topographic GWD parameterization. With his GWD parameterization the simulated circulation is similar to that obtained by HWMU (i.e., somewhat realistic, but still affected by the polar cold bias above the middle stratosphere).

In the SH winter, the polar middle atmospheric cold bias has been an even more severe and intractable problem. Once again, in the SH the topographic GWD is unlikely to be important, and models produce very cold SH polar simulations whether or not they include a topographic GWD parameterization (Boville 1991; HWMU; Hamilton 1995). Simulations performed with low-resolution climate models (e.g., Fels et al. 1980) may have polar temperatures ~100°C too cold near the stratopause and peak zonal mean zonal winds in the mesosphere exceeding 200 m s^{-1}. It seems likely that the basic explanation for this deficiency in the models is the inability to resolve an important component of the spectrum of nonstationary gravity waves excited by various tropospheric processes. Garcia and Boville (1994) show that a plausible parameterization of the zonal drag associated with unresolved nonstationary gravity waves can produce a realistic simulation in a simple mechanistic model of the middle atmospheric circulation. Currently there are efforts underway to include such GWD schemes in full GCMs. Unfortunately, parameterizations of the subgrid-scale GWD have to be formulated in the face of serious inadequacies in the detailed knowledge of the gravity wave field in the real atmosphere. One obvious question to consider is how well GCMs can perform if run at a high enough resolution to explicitly resolve a significant fraction of the gravity wave spectrum. HWMU present some encouraging results in this regard. They found that the June–August mean SH cold pole bias near the stratopause was ~65°C in a version of their model with ~300-km grid spacing, but declined to ~35°C when the grid spacing was reduced to ~100 km. The peak June–August mean zonal-mean zonal winds in these two simulations were found to be ~190 m s^{-1} and ~130 m s^{-1}, respectively [compared to observations of ~80 m s^{-1}, e.g., Fleming et al. (1988)].

HWMU found that both the surface wind bias and the cold winter pole bias were strongly affected by horizontal model resolution, and they found no evidence that the dependence of the model climatology on resolution had converged even at ~100-km grid spacing. The present paper reports on a further investigation of these issues through analysis of results from a very high horizontal resolution (~60-km spacing), 40-level global GCM. Integration of such a model is computationally expensive, so the simulation was limited to a period of about 2 months. In order to study the SH winter simulation, the integration was performed over a period from early May through early July. Comparisons will be made with lower resolution simulations with the same model. Of particular interest will be comparisons with the highest resolution (~100 km) version considered by HWMU, for which there are now several years of simulation available. The GCM used is briefly described in section 2, below. Section 3 discusses the results for both the troposphere and middle atmosphere. The conclusions are summarized in section 4.

2. Model and integrations

The Geophysics Fluid Dynamics Laboratory SKYHI model is described in Fels et al. (1980) and HWMU. It is a comprehensive, primitive equation, gridpoint GCM designed to simulate the global atmosphere from the ground to near the mesopause. In all the experiments discussed in HWMU and in this paper, a hybrid sigma-pressure coordinate with 40 levels in the vertical is employed. At the top of the domain the usual ''rigid lid'' boundary condition (i.e., the pressure velocity is zero at zero pressure) is used. There is also a strong linear damping of all fields at the highest full model level (0.0096 mb) that is applied only to the deviations from the zonal mean (see Fels et al. 1980) and thus does not directly act on the mean circulation. The model has a sophisticated radiative transfer code that is used to compute diurnally averaged shortwave heating rates (see HWMU for details) as well as instantaneous longwave heating rates. Mean ozone amounts are prescribed, but locally the mixing ratio is allowed to vary linearly with temperature in order to account for the photochemical acceleration of radiative eddy damping (see Fels et al. 1980). The cloud field used for the radiative transfer calculations in the model is also prescribed. The hydrologic cycle is included by very simple parameterizations of runoff, evaporation, moist convection, and stable precipitation. A dry convective adjustment and a Richardson number-dependent vertical diffusion are also employed. A nonlinear horizontal subgrid-scale diffusion is included (Andrews et al. 1983).

In HWMU, integrations with three different latitude–longitude resolutions are described: 3° × 3.6° (N30), 2° × 2.4° (N45), and 1° × 1.2° (N90), where the ''N'' notation refers to the number of grid rows between the equator and pole (note that in each case a zonal Fourier filter is applied at latitudes poleward of about 45° lat in

order to preserve a roughly isotropic effective resolution). Using the notation for the numbering of years described in HWMU, the N90 control integration starts in October 1982 and has now continued into July 1985, but with a significant change in the model physics introduced on 1 May 1983 (details can be found in HWMU). In addition, another parallel integration was undertaken with the same model, using initial conditions from the control run on 8 March 1985, but which were randomly perturbed in the troposphere (following essentially the procedure used in the predictability experiments described in Hamilton 1994). This integration proceeded into July, yielding another realization of the N90 June circulation (referred to here as ''1985A''). The N90 results shown in the present paper are based on the June 1984, 1985, and 1985A N90 simulations, with the June 1983 period excluded due to possible contamination from the changes in model physics introduced at the beginning of May. Note, however, that the basic results described below are essentially unchanged when the June 1983 N90 period is also included.

The present paper introduces the first results obtained with the N150 ($0.6° \times 0.72°$) version of SKYHI. This version of the model has very challenging computational requirements. The present integration was performed on the massively parallel CM5 computer system at Los Alamos National Laboratory. The technical issues involved in the adaptation of the model code for the CM5 architecture are described in Jones et al. (1995). Practical considerations limited the integration to a roughly 2-month period. The N150 simulation began with initial conditions interpolated in a simple manner from the N90 control experiment on 5 May 1984 and continued through 3 July of that year. The model was run with the same prescribed sea surface temperatures as in the N90 control. The first few days of the N150 simulation included some extra damping on the deviations from the zonal mean imposed in the top levels in order to dissipate the gravity waves produced from the initialization. The topography employed in the N150 model was interpolated from the N90 topography to make the N90 and N150 topographic heights as consistent as possible (a point of interest later in the discussion of the present results). Note that the N90 topography itself is essentially unsmoothed (except poleward of ~45° lat, where a polar filter is applied in the zonal direction to make the topography consistent with the treatment of model dynamics).

3. Results

Figure 1 shows the results for the simulated June average zonal mean temperature. Figure 1a is the temperature as simulated in the single N150 realization, and Fig. 1b is the difference with the observed climatology of Fleming et al. (1988). It is apparent that the cold winter polar bias is present in the model, particularly in the upper stratosphere and lower mesosphere, where there is a large region in which the simulated temperatures are ~15°–20°C colder than observed. The difference between the N150 and N90 simulated zonal mean temperatures is shown in Fig. 1c. The N150 simulation near the winter pole is a considerable improvement over that at N90, by as much as 10°C near 1 mb. Thus the improvement in the SH winter middle atmospheric circulation with finer resolution seen in the N30, N45, and N90 simulations of HWMU appears to continue at least up to the N150 version. The N150 minus N90 temperature difference normalized by the standard deviation of the three monthly mean N90 June realizations is displayed in Fig. 1d. This shows that the warm polar temperatures in the N150 simulation do indeed stand out clearly from the ensemble of N90 realizations.

There are some additional features in Fig. 1 that are of interest. The reader will note that the tropospheric temperatures in the N150 experiment appear to be ~5°C colder than observed. This is a bias that has been noted earlier in HWMU and is likely attributable to deficiencies in the cloud field in the model. Or, put another way, this deficiency could be largely eliminated by prescribing some additional upper-tropospheric cirrus clouds. This bias is particularly severe near the tropical tropopause, but here it is seen to slightly decrease at N150 relative to N90. The warming of ~1°C seen at the tropical tropopause level in N150 (Fig. 1c) is actually more than six times the N90 standard deviation (Fig. 1d). Again this tendency for the upper tropical troposphere to warm with increasing resolution was seen by HWMU for the N30, N45, and N90 simulations. The simulated extratropical summer middle atmosphere also shows some dependence on resolution.

As noted in HWMU, the temperatures in the summer polar upper mesosphere in SKYHI are warmer than actually observed. This is the summer analog of the winter ''cold pole'' problem and again reflects a simulation that has unrealistically weak eddy forcing of the mean flow (and hence is too close to radiative equilibrium). HWMU noted that the warm bias in the summer polar mesosphere also improved somewhat as the horizontal resolution was increased from N30 to N90. The results for the June N150 temperatures do not appear to show continued improvement in this regard. In fact, the June North Pole temperatures at the top level are actually warmer by ~4°C in the N150 simulation. On the other hand, there is a cooling in the N150 simulation relative to the N90 simulation by ~1°C in the NH high latitudes in a deep layer below about 0.1 mb. This is associated with a summertime easterly jet that is actually weaker in N150 than in N90 (see Fig. 2).

The N150 minus N90 zonal mean temperatures were computed separately for two shorter periods: 28 May–15 June and 16 June–3 July. The results for these two periods (not shown) are actually quite similar. This is reassuring, both in terms of confirming the significance of the differences seen in Fig. 1b and also in suggesting that the results by late May are not strongly affected by

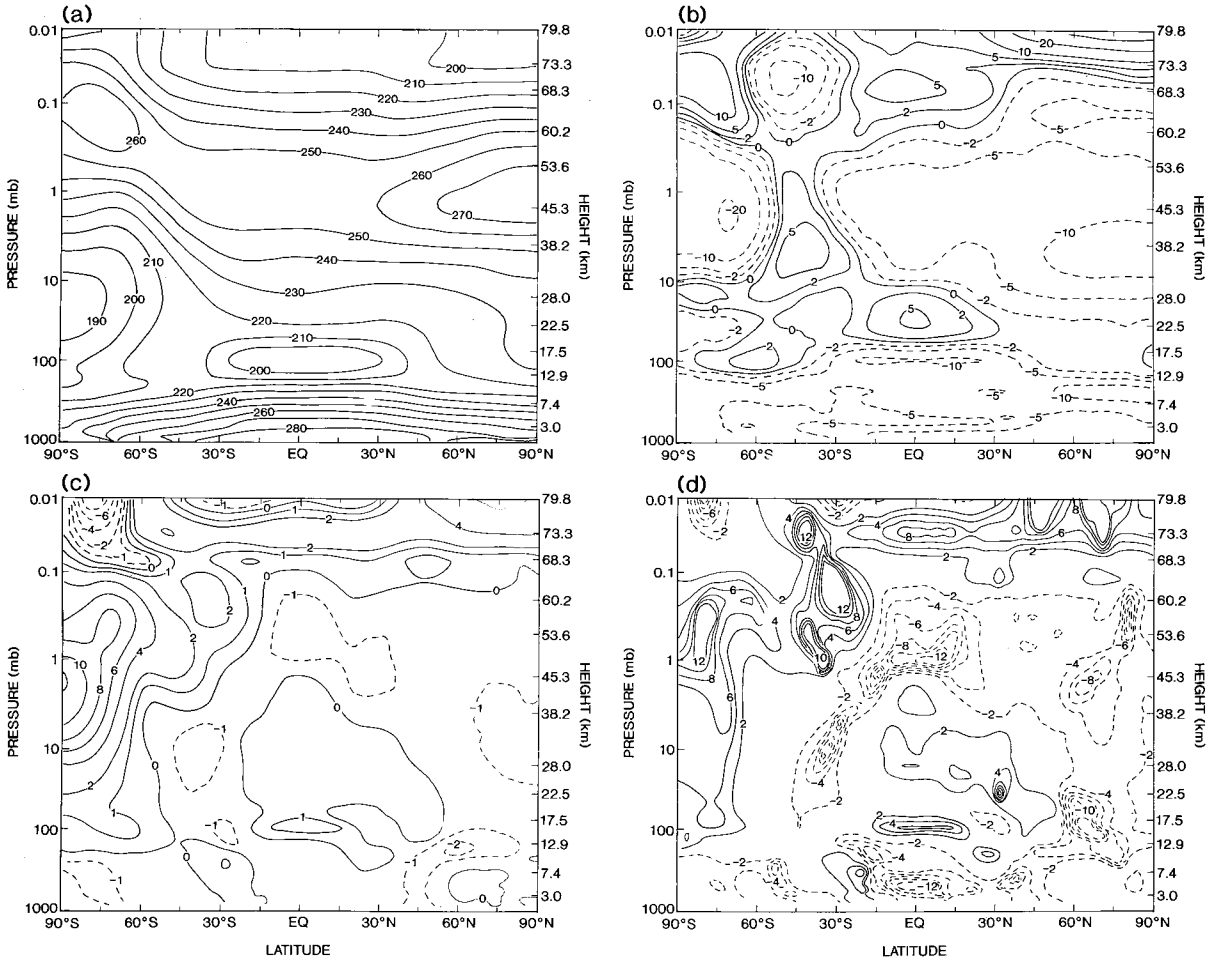

FIG. 1. (a) June average zonal mean temperature in the N150 integration. Contour labels in °C. (b) Difference of the N150 temperatures from the June climatology of Fleming et al. (1988). Dashed contours indicate regions where the N150 results are colder. Contours plotted for 0°, ±2°, ±5°, ±10°, ±20°C, etc. (c) Difference of the June N150 temperatures from the mean of three N90 integrations. Dashed contours indicate regions where the N150 results are colder. Contours plotted for 0°, ±1°, ±2°, ±4°, ±6°C, etc. (d) The difference between N150 and N90 temperatures normalized by the standard deviation of the June temperatures in the three N90 realizations. No zero contour is plotted. In (b), (c), and (d), dashed contours indicate regions where the N150 results are colder. In this and subsequent figures, the heights shown on the axis are for a standard midlatitude atmospheric profile.

any initial adjustment of the model from the N90 to N150 versions.

Figure 2 summarizes results for the June average-zonal mean zonal wind. The N150 simulation has a strong westerly middle-atmospheric vortex around the winter pole that is unrealistically strong (>110 m s^{-1}, vs ~80 m s^{-1} in observations) and confined unrealistically near the pole. The net effect is a simulated wind field that can be as much as ~50 m s^{-1} different at some locations from the observations reported in Fleming et al. (1988). However, this N150 simulation is still a considerable improvement over that at N90 (not shown) and is very much improved over lower resolution simulations obtained with the SKYHI model. Even the observed equatorward tilting of the vortex edge with height in the mesosphere is captured to some extent in this N150 simulation (but not in any other published GCM simulation of the SH winter circulation). Figure 2b shows the difference in the June average zonal mean zonal winds between the N150 and N90 simulations. The reduction in the strength of the polar middle atmospheric vortex in the N150 model is evident. In addition, there are large (~10 m s^{-1}) differences in the middle-atmospheric equatorial winds. However, there is no reason to believe that these changes in the Tropics have in fact equilibrated during the brief N150 integration (e.g., Mahlman and Umscheid 1984; Hamilton and Yuan 1992). Also noteworthy in Fig. 2b are the large differences in the zonal wind in the SH troposphere, with increased westerlies at high latitudes and stronger easterlies or weaker westerlies equatorward of about 30° lat. The tropospheric aspects of the simulation will be addressed in more detail below.

Figure 2c shows the N150 minus N90 zonal wind

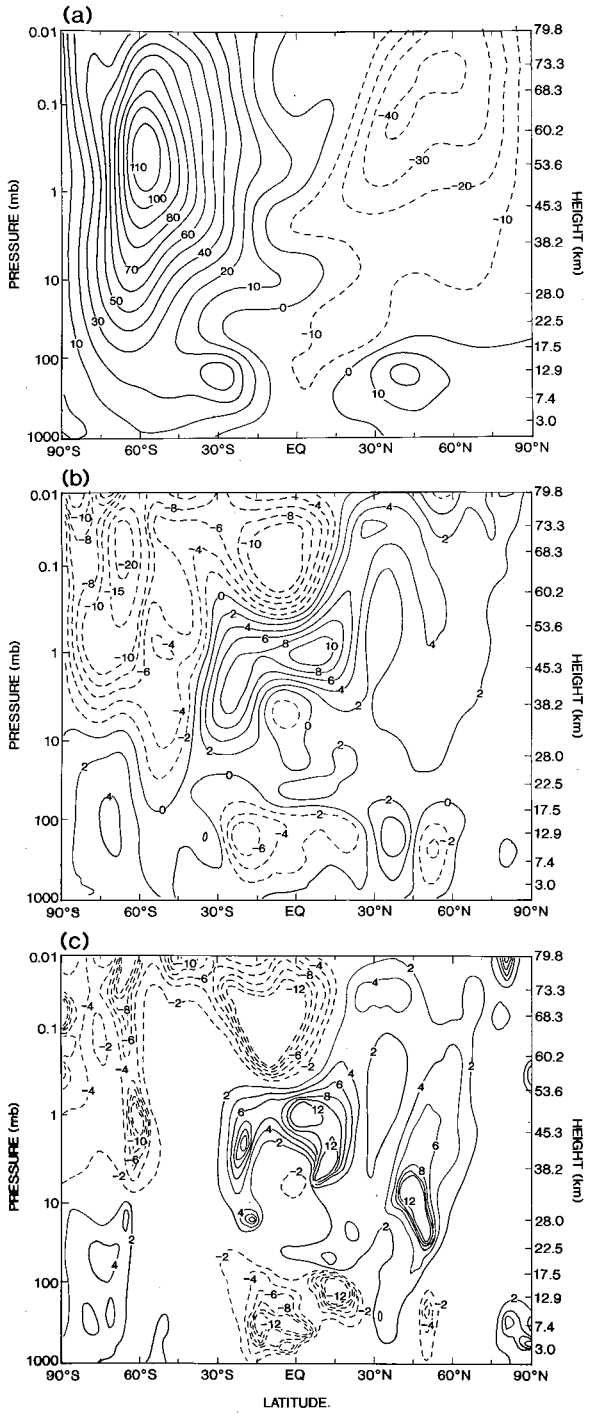

FIG. 2. (a) June average zonal mean zonal wind in the N150 integration. Dashed contours denote easterly winds, and contours are labeled in m s^{-1}. (b) Difference of the zonal wind in the N150 integration from the June climatology of the N90 integrations. (c) The difference between N150 and N90 zonal winds normalized by the standard deviation of the June zonal winds in the three N90 realizations. No zero contour is plotted.

difference normalized by the standard deviation of the three individual monthly mean N90 June realizations. This again suggests that the N150 results do stand out from those at N90, particularly near the vortex edge, in the tropical middle atmosphere, and in the tropospheric tropical and winter polar regions.

Figure 3 summarizes the results for the eddy forcing of the mean flow, here determined as the Eliassen–Palm flux divergence normalized in the usual fashion to be in acceleration units (referred to hereafter as EPFD; see Andrews et al. 1983). The June average results for N90 and N150 are shown as Figs. 3a and 3b, respectively, while the difference is displayed in Fig. 3c. In N90 and N150, the EPFD clearly acts as a brake on both the winter westerly vortex and the easterly summer vortex. The extratropical winter EPFD in N150 is obviously different from that at N90 with significantly more easterly drag appearing throughout the middle atmosphere (except right at the top level). This is consistent with the drag being produced largely by explicitly resolved gravity waves. Such waves are forced in the model by tropospheric convection (examined in detail by Manzini and Hamilton 1993) and by other nonlinearities of the flow. Earlier experience with the SKYHI model has shown that as the horizontal resolution is increased, the spectrum of gravity waves fills out so that there is significant wave activity at all resolved wavenumbers (e.g., Hayashi et al. 1989; Hamilton 1993, 1995; Hayashi and Golder 1994). The wave amplitudes at the lower end of the wavenumber spectrum also tend to increase with resolution. The result is to produce both stronger wave amplitudes and more gravity wave momentum flux in the mesosphere. This leads to stronger mean flow forcing from the waves and, since the stronger wave activity allows waves to break lower down, a tendency for the wave drag on the mean flow to extend to lower levels. The tendency for waves to break lower down may account for the SH easterly drag at the top level of the model (~0.01 mb) to be somewhat weaker in the N150 model. Also computed was the difference field in Fig. 3c normalized by the standard deviation of the three N90 realizations (not shown). The large differences seen in Fig. 3c in the upper mesosphere of both the SH and NH are between about two and six times the N90 standard deviation. The large differences in the high-latitude SH between about 50 mb and 0.5 mb are generally more than 10 times the N90 standard deviation.

Figure 3d displays the EPFD calculated from the June average fields of the N150 integration and represents a simple attempt to isolate the contribution from quasi-stationary eddies (largely zonal wave one). The result is quite striking, with a substantial fraction of the total EPFD in the SH below 5 mb accounted for by the monthly mean. By contrast, the stationary waves make almost no contribution to the EPFD in the N90 simulation. It seems likely that the increased drag from the gravity waves at N150 has sufficiently altered the mean

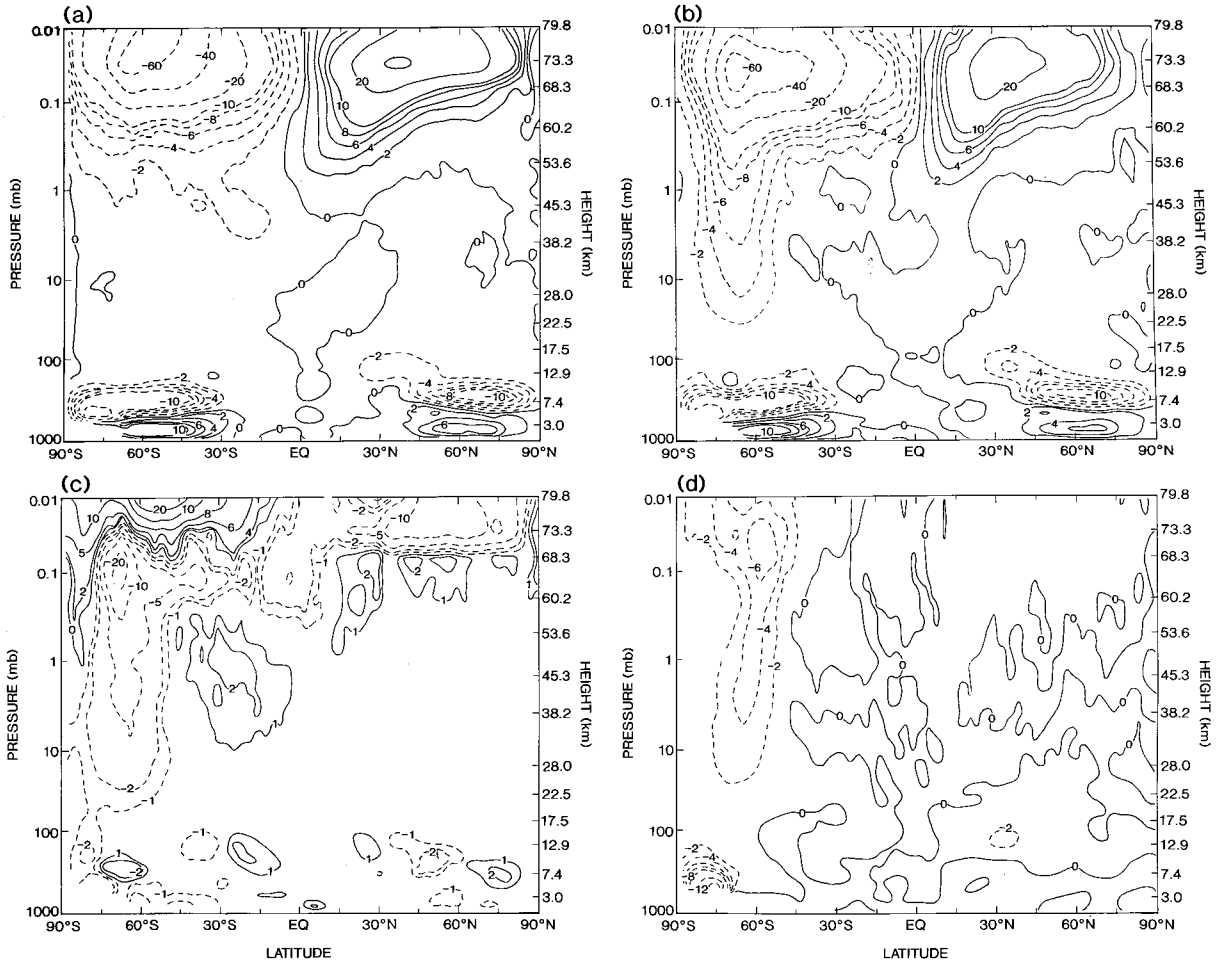

FIG. 3. (a) June average force/unit mass due to the Eliassen–Palm flux divergence in the N90 integration. Contours labeled in m s^{-1} day^{-1} and plotted for values of 0°, ±2, ±4, ±6, ±8, ±10, ±20, ±40, etc. Dashed contours denote easterly forcing of the mean flow. (b) As in (a) but for the N150 climatology. (c) Difference between the N150 and N90 results. (d) N150 results for the stationary component (i.e., when calculated using the June average fields).

flow distribution to allow some stationary wave Eliassen–Palm flux penetration into the middle stratosphere.

One important limitation in the present N150 middle-atmospheric simulation is the restriction to the early SH winter period. As the winter progresses, the radiative effects in the polar night could act to force a colder polar middle atmosphere (possibly offset by increased planetary wave activity in the troposphere as winter progresses). The fact that the N150 SKYHI model can produce a June average polar stratopause only ~20°C colder than observed does not guarantee that comparably good results would be obtained later in the winter.

As noted above, the tropospheric zonal mean wind field appears to be considerably changed in N150 from that at N90. Poleward of about 45° lat the tropospheric westerly winds are increased, with the westerlies at the lowest model level (~80 m above the surface) increased by more than 2 m s^{-1}. Figure 4 compares the N150 simulated June average sea level pressure (SLP) with that based on 8 years of European Centre for Medium-Range Weather Forecasts daily observational analyses (Schubert et al. 1990). The simulated SLP gradients are obviously much stronger than observed, particularly poleward of about 50°S. Figure 5 is a comparison of the June average zonal mean surface pressure in the N150 run with those for individual years in the N90 run (note that no correction to SLP is applied). The results in each case are presented as deviations from the average over all three June periods for N90. The pressure anomaly shown for the N150 run drops ~17 mb between 50°S and 85°S, and ~8 mb between 50°S and 65°S, indicating that the meridional pressure gradients are more intense in the N150 integration than in the average of the 3 N90 years (note that the topography in the N90 and N150 runs is as consistent as possible, which makes the direct comparison of surface pressures in the two models meaningful). The spread among the individual N90 curves in Fig. 5 is an indication of the significant interannual variability in this simulation, but the N150 results do appear to stand out clearly from the N90

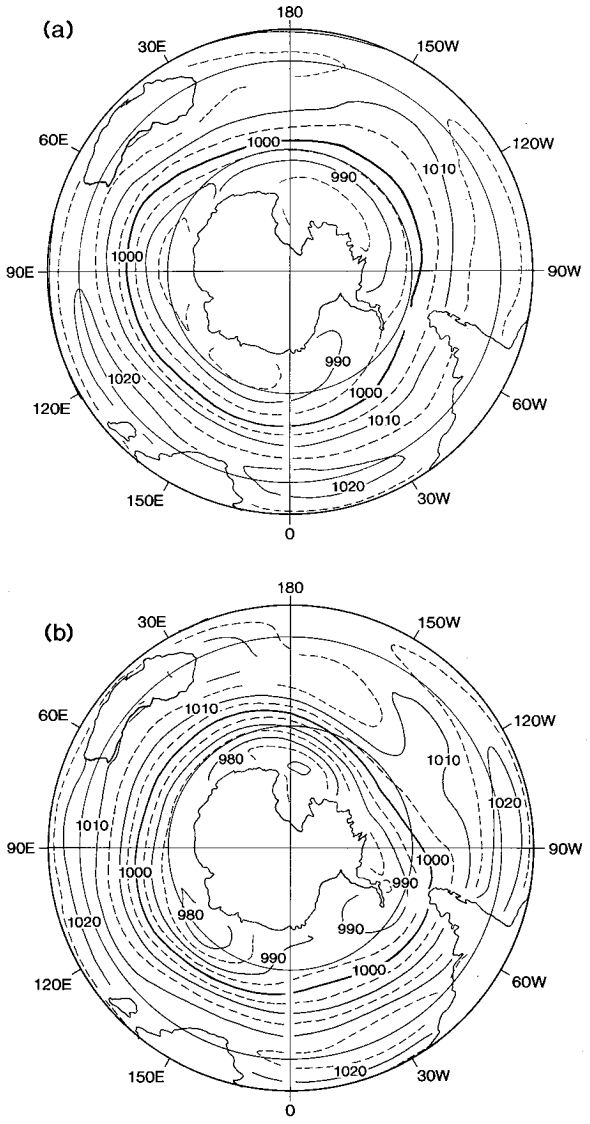

FIG. 4. (a) Observed June average sea level pressure for the SH. Data from Schubert et al. (1990). Contours are labeled in mb. The contour interval is 5 mb, and dashed contours alternate with solid contours. (b) June average sea level pressure from the N150 SKYHI integration. In each case the contours are not plotted anywhere that the N150 topography exceeds 50 m. Results presented in an orthonormal projection. The latitude circles shown are at 30°S and 60°S.

realizations. Note that even at N90 resolution, the SKYHI SH winter SLP gradients poleward of 50°S are unrealistically intense (HWMU). This problem has become exacerbated at N150 resolution (at least in June).

Figure 6 shows the meridional eddy transport of zonal momentum (normalized by the density) for the N150 June and the difference field between this value and the N90 June climatology (note that only the troposphere and lower stratosphere is displayed). In the SH the total transport is poleward at almost all latitudes, and the transport is substantially larger for N150 than for N90. This increase in eddy momentum flux is consistent with the trend seen in lower resolution versions of SKYHI (HWMU) and in other models (Held and Phillips 1993). The increased meridional momentum flux has to be balanced by surface friction in the high latitudes, and so the changes in momentum flux are closely connected with the changes seen in surface winds and surface pressure gradients. The peak June N150 momentum transports in the SH shown in Fig. 6 are somewhat stronger than the observational estimates for June–August given by Oort (1983) and Schubert et al. (1990). However, the biggest difference is at high latitudes, where the observations actually indicate a region of equatorward eddy momentum fluxes, while in the N150 simulation the fluxes are poleward even at high latitudes.

4. Discussion and conclusions

This paper has examined an integration obtained with a global GCM with very fine horizontal resolution, as well as comparisons with results from lower resolution versions of the same model. While the experiments and analysis discussed are quite straightforward, the results touch on some fundamental issues in the study of the general circulation of the atmosphere. The tendency for the poleward eddy momentum transport and the meridional surface pressure gradients in extratropical SH winter hemisphere to increase with resolution is quite apparent in these results. There seems to be no indication that this process has converged, and it may be that even further deterioration of the simulation would be found at higher resolutions. This is a rather basic issue for the modeling of the SH winter circulation and also must raise the issue of whether the imposition of topographic gravity wave drag in the NH actually represents an important effect in the real atmosphere, or merely masks the same fundamental problem (i.e., a tendency for the model to overpredict the poleward tropospheric eddy momentum transports; see Klinker and Sardeshmukh 1992).

It is not clear whether the SKYHI results for the surface pressure gradients would be representative of other GCMs if run at very high resolution. Boyle (1993) discussed climate simulations with the spectral European Centre for Medium-Range Weather Forecasts model run at different resolutions up to T106 truncation (which might be considered roughly comparable to the N90 grid resolution). He mostly shows the boreal winter results, but does state that in June–August the peak SH eddy momentum transports and the overall sea level pressure distribution do not change dramatically after resolution is increased above T42 (the SH winter momentum fluxes at high resolution in his model are apparently somewhat larger than observed, just as in SKYHI). It is also interesting to note that the zonally averaged surface zonal winds near 60°S in Boyle's December–February simulations do show a significant increase with resolution (by $\sim$2 m s^{-1}) between T62 and T106. Also relevant are the recent papers of Held and Suarez (1994) and

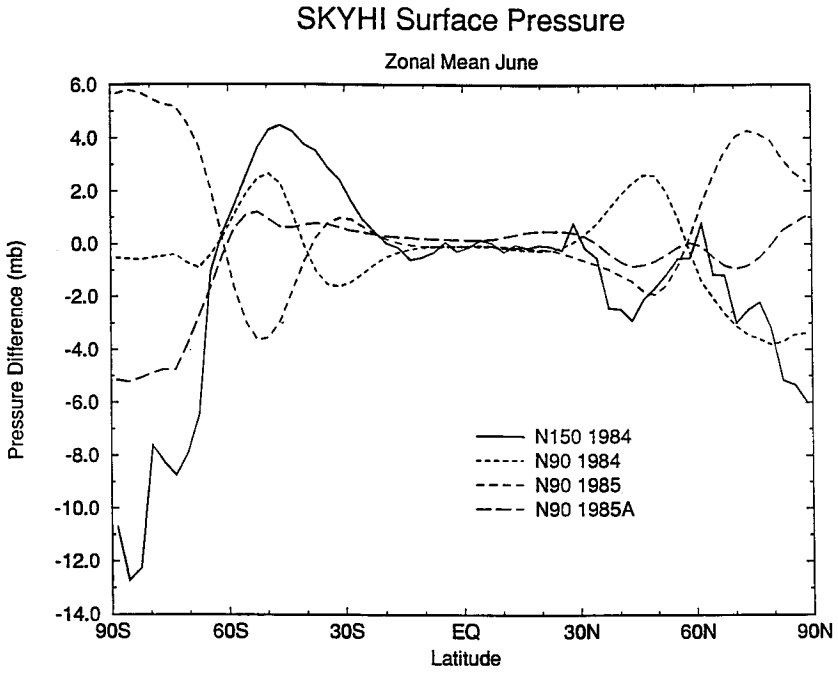

FIG. 5. The deviation of the June average zonal mean surface pressure from the average of that obtained in the three N90 realizations. The solid curve is for the N150 integration, while the other three curves are for each of the N90 June realizations separately.

Boer and Denis (1996) examining the behavior of three-dimensional global models idealized to include no moisture or topography and to have simplified radiative forcing. Boer and Denis, using a spectral model, found little sensitivity of the surface pressure distribution to increases in horizontal resolution above triangular-63. Held and Suarez do not present results for the surface pressure, but find a generally slower convergence of the circulation with resolution than do Boer and Denis. Held and Suarez also note that spectral models seem to converge somewhat faster than gridpoint models.

The results of the N150 simulation in the SH winter middle atmosphere are quite encouraging. The Eliassen–Palm flux divergence (EPFD) from explicitly resolved waves is increased at N150 over that at N90 throughout the extratropical SH, and this leads to a warmer winter pole and a more realistic vortex. While there are still very considerable deficiencies in the N150 SH winter simulation, the present results do suggest that a significant fraction of the EPFD associated with gravity waves in the middle atmosphere may be in the horizontal spectrum range from ~100 to ~1000s of km. This is an important issue for the formulation of subgrid-scale GWD parameterizations for GCMs, which all require some specification of the spectrum of waves emerging from the troposphere (e.g., Lindzen 1981; Hines 1996). More detailed analysis of the explicitly resolved middle atmospheric wave field in the present N150 simulation is now underway (Y. Hayashi 1996, personal communication).

The present paper has concentrated on comparing results from the two highest horizontal resolution SKYHI simulations available (N90 and N150). However, it is important to emphasize that the major differences seen between the N150 and N90 models represent a continuation of trends found at lower resolution (documented in HWMU). It is also striking that the resolution dependence of neither the middle-atmospheric polar vortex simulation nor the high-latitude surface winds shows any apparent tendency to converge, even in the N150 version.

The present results raise a large number of related questions. Obviously the sensitivity of the results to vertical resolution and to changes in model physics needs to be investigated further. There have been at least two studies of the effects of increasing vertical resolution within middle-atmospheric GCMs beyond the ~2 km considered in the present model experiments. Boville and Randel (1992) looked at a simulation with different vertical level spacings (~3 km down to ~0.7 km) throughout the middle atmosphere in a T21 resolution spectral GCM, while Hamilton and Yuan (1992) compared simulations conducted with a rhomboidal-15 truncation GCM with ~2-km and ~2/3-km vertical level spacing. Neither of these studies found any very dramatic modification of the extratropical circulation with increased vertical resolution, although Boville and Randel found some interesting resolution dependence of the simulated structure of the semiannual oscillation near the tropical stratopause. There is still much to be done in this regard, however. In particular, the effects of enhanced vertical resolution has only been investigated in

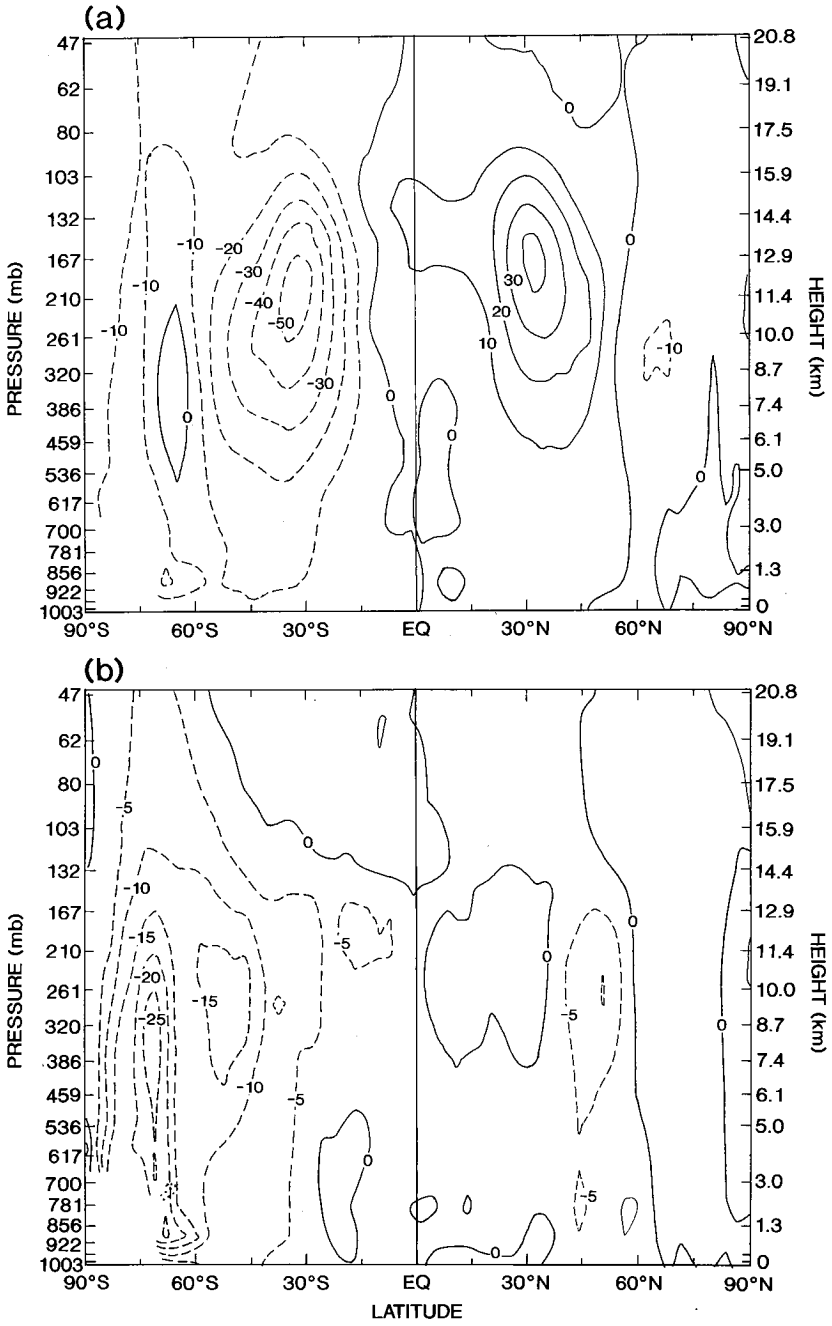

FIG. 6. (a) Meridional transport of zonal momentum per unit mass by eddies in the N150 integration. June average results are shown. The contours are labeled in $m^2 s^{-2}$, and negative values (dashed contours) indicate southward transport of westerly momentum. (b) The June average eddy momentum transport in the N150 experiment minus that averaged for the three N90 June realizations. Negative values (dashed contours) indicate regions where there is more southward transport of westerly momentum in the N150 results. The eddy component here is defined as any deviation from the zonal mean.

models with rather coarse horizontal resolution. Presumably as horizontal resolution is increased, a point is reached at which more benefit will result from improvement in the vertical resolution.

The question of how model results may change with alterations in the subgrid-scale parameterizations also needs to be addressed. Unfortunately, extensive sensitivity experiments with the very high resolution model considered in this paper are not practical at present. There are some aspects that might be profitably ex-

amined at somewhat lower resolution, however. The dependence of the low-level winds and SLP gradients on the formulation of surface drag could be examined, for example. The effects of changing the subgrid-scale mixing parameterizations on the strength of the simulated tropospheric eddy momentum transports is another obvious issue for investigation.

Acknowledgments. The support of Jerry Mahlman and Bob Malone throughout this project is greatly appreciated. Richard Hemler and Christopher Kerr assisted in the code changes needed to run the model on the CM5, and Don Golder assisted in the initial evaluation of the model integrations. Tony Broccoli, Yoshi Hayashi, Jerry Mahlman, and the official reviewers provided helpful comments on the manuscript. We gratefully acknowledge the Advanced Computing Laboratory of Los Alamos National Laboratory, where the high-resolution simulations were carried out. This work was supported in part by the Department of Energy's Computer Hardware, Advanced Mathematics, and Model Physics Program for Climate Studies.

REFERENCES

Andrews, D. G., J. D. Mahlman, and R. W. Sinclair, 1983: Eliassen–Palm diagnostics of wave-mean flow interaction in the GFDL ''SKYHI'' general circulation model. *J. Atmos. Sci.,* **40,** 2768–2784.

Boer, G. J., and M. Lazare, 1988: Some results concerning the effect of horizontal resolution and gravity-wave drag on simulated climate. *J. Climate,* **1,** 789–806.

——, and B. Denis, 1996: Numerical convergence of the dynamics of a GCM. *Climate Dyn.,* in press.

Boville, B. A., 1991: Sensitivity of the simulated climate to model resolution. *J. Climate,* **4,** 469–485.

——, and W. J. Randel, 1992: Equatorial waves in a stratospheric GCM: Effects of vertical resolution. *J. Atmos. Sci.,* **49,** 785–801.

Boyle, J. S., 1993: Sensitivity of dynamical quantities to horizontal resolution for a climate simulation using the ECMWF (cycle 33) model. *J. Climate,* **6,** 796–815.

Fels, S. B., J. D. Mahlman, M. D. Schwarzkopf, and R. W. Sinclair, 1980: Stratospheric sensitivity to perturbations in ozone and carbon dioxide: Radiative and dynamical responses. *J. Atmos. Sci.,* **37,** 2265–2297.

Fleming, E. L., S. Chandra, M. R. Schoeberl, and J. J. Barnett, 1988: Monthly mean global climatology of temperature, wind, geopotential height, and pressure for 0–120 km. NASA Tech. Memo. 100697, 85 pp. [Available from NASA/Goddard Space Flight Center, Greenbelt, MD 20771.]

Garcia, R. R., and B. A. Boville, 1994: ''Downward control'' of the mean meridional circulation and temperature distribution of the polar winter stratosphere. *J. Atmos. Sci.,* **51,** 2238–2245.

Hamilton, K., 1993: What we can learn from general circulation models about the spectrum of middle atmospheric motions. *Coupling Processes in the Lower and Middle Atmosphere,* E. Thrane, T. Blix, and D. Fritts, Eds., Kluwer Academic Publishers, 161–174.

——, 1994: The GFDL SKYHI model: Results of relevance for numerical weather prediction. *The Stratosphere and Numerical Weather Prediction,* A. Simmons, Ed., European Centre for Medium-Range Weather Forecasts, 213–231.

——, 1995: Comprehensive modelling of the middle atmospheric climate: Some recent results. *Climate Dyn.,* **11,** 223–241.

——, and L. Yuan, 1992: Experiments on tropical stratospheric mean wind variations in a spectral general circulation model. *J. Atmos. Sci.,* **49,** 2464–2483.

——, R. J. Wilson, J. D. Mahlman, and L. J. Umscheid, 1995: Climatology of the SKYHI troposphere–stratosphere–mesosphere general circulation model. *J. Atmos. Sci.,* **52,** 5–43.

Hayashi, Y., and D. G. Golder, 1994: Kelvin and mixed Rossby–gravity waves appearing in the GFDL SKYHI general circulation model and the FGGE dataset: Implications for the generation mechanism and role in the QBO. *J. Meteor. Soc. Japan,* **72,** 901–935.

——, J. D. Mahlman, and S. Miyahara, 1989: The effect of horizontal resolution on gravity waves simulated by the GFDL SKYHI general circulation model. *Pure Appl. Geophys.,* **130,** 421–443.

Held, I. M., and P. J. Phillipps, 1993: Sensitivity of the eddy momentum flux to meridional resolution in atmospheric GCMs. *J. Climate,* **6,** 499–507.

——, and M. J. Suarez, 1994: A proposal for the intercomparison of the dynamical cores of atmospheric general circulation models. *Bull. Amer. Meteor. Soc.,* **75,** 1825–1830.

Hines, C. O., 1996: Parameterization of gravity wave momentum deposition in the middle atmsophere. Part I: Continuous spectrum of extrowaves. *J. Atmos. Terr. Sci.,* **59,** 371–386.

Jones, P. W., C. L. Kerr, and R. S. Hemler, 1995: Practical considerations in development of a parallel SKYHI general circulation model. *Parallel Comput.,* **21,** 1677–1694.

Lindzen, R. S., 1981: Turbulence and stress due to gravity wave breakdown. *J. Geophys. Res.,* **86,** 9707–9714.

Klinker, E., and P. D. Sardeshmukh, 1992: The diagnosis of mechanical dissipation in the atmosphere from large-scale balance requirements. *J. Atmos. Sci.,* **49,** 608–627.

Mahlman, J. D., and L. J. Umscheid, 1984: Dynamics of the middle atmosphere: Successes and problems of the GFDL ''SKYHI'' general circulation model. *Dynamics of the Middle Atmosphere,* J. R. Holton and T. Matsuno, Eds., Terra Scientific, 501–525.

Manabe, S., D. G. Hahn, and J. L. Holloway, 1979: Climate simulations with GFDL spectral models of the atmosphere: Effects of spectral truncation. Rep. JOC Study Conf. on Climate Models: Performance, Intercomparison and Sensitivity Studies, Vol. 1, GARP Publ. 22. [Available from World Meteorological Organization, Case Postale No. 2300, CH-1211 Geneva 2, Switzerland.]

Manzini, E., and K. Hamilton, 1993: Middle atmospheric travelling waves forced by latent and convective heating. *J. Atmos. Sci.,* **50,** 2180–2200.

McFarlane, N. A., 1987: The effect of orographically excited gravity-wave drag on the general circulation of the lower stratosphere and troposphere. *J. Atmos. Sci.,* **44,** 1775–1800.

Oort, A. H., 1983: Global atmospheric circulation statistics, 1958–1973. NOAA Prof. Paper 14, 180 pp.

Palmer, T. N., G. J. Shutts, and R. Swinbank, 1986: Alleviation of a systematic westerly bias in general circulation and numerical weather prediction models through an orographic gravity wave parameterization. *Quart. J. Roy. Meteor. Soc.,* **112,** 1001–1039.

Schubert, S., S. Moorthi, C.-K. Park, M. Suarez, and W. Higgins, 1990: An atlas of ECMWF analyses—Part I. NASA Tech. Memo. 100747. [Available from NASA/Goddard Space Flight Center, Greenbelt, MD 20771.]